Effect of Interfacial Stress on the Crystalline Structure of the Matrix and the Mechanical Properties of High-Density Polyethylene/$CaCO_3$ Blends

Yuncan Zhang,[1,2] Enli Pan[2]

[1]*State Key Laboratory of Polymer Material Engineering, Polymer Research Institute of Sichuan University, Chengdu 610065, China*
[2]*Department of Polymer Material Science and Engineering, Nanjing University of Chemical Technology, Nanjing 210009, China*

Received 11 October 2001; accepted 13 May 2002

ABSTRACT: A series of high-density polyethylene (HDPE)/$CaCO_3$ blends were prepared with different kinds of coupling agents, with $CaCO_3$ particles of different sizes, and with matrixes of different molecular weights during the melt-mixing of HDPE and $CaCO_3$ particles. The mechanical properties of these blends and their dependence on the interfacial adhesion and matrix crystalline structure were studied. The results showed that the Charpy notched impact strength of these blends could be significantly improved with an increase in the interfacial adhesion or matrix molecular weight or a decrease in the $CaCO_3$ particle size. When a $CaCO_3$ surface was treated with a compounded coupling agent, the impact strength of the HDPE/$CaCO_3$(60/40) blend was 62.0 kJ/m^2, 2.3 times higher than that of unimproved HDPE; its Young's modulus was 2070 MPa, 1.07 times higher than that of unimproved HDPE. The heat distortion temperature of this blend was also obviously improved. The improvement of the mechanical properties and the occurrence of the brittle–tough transition of these blends were the results of a crystallization effect induced by the interfacial stress. When the interfacial adhesion was higher and the $CaCO_3$ content was greater than 30%, the interfacial stress produced from matrix shrinkage in the blend molding process could strain-induce crystallization of the matrix, leading to an increase in the matrix crystallinity and the formation of an extended-chain (or microfibrillar) crystal network. The increase in the critical ligament thickness with an increasing matrix molecular weight was attributed to the strain-induced areas becoming wider, the extended-chain crystal layers becoming thicker, and the interparticle distance that formed the extended-chain crystal network structure becoming larger with a higher matrix molecular weight. The formation of the extended-chain crystal network and the increase in the matrix crystallinity were also the main reasons that Young's modulus and the heat distortion temperature of this blend were improved. © 2003 Wiley Periodicals, Inc. J Appl Polym Sci 87: 2120–2129, 2003

Key words: polyethylene (PE); stress; brittle; toughness; networks

INTRODUCTION

The appropriate incorporation of rubber particles into a brittle plastic matrix has led to an important class of commercial polymers, including high-impact polystyrenes and acrylonitrile–butadiene–styrene copolymer resins.[1] Under proper conditions, the addition of rubber to semiductile thermoplastics, such as certain polyamides, polyesters, and polypropylenes, has led to a class of supertough blends.[2–9] However, the enhancement of both the impact strength and the modulus of some semiductile polymers by the introduction of nonelastomers, that is, plastics and inorganic fillers, has also been achieved and commercially developed.[10–17] Therefore, the toughening mechanism of these systems is attracting much attention.

Generally, the popularly accepted view of the mechanism is that the dispersed particles act as stress concentrators to initiate and terminate crazes in the brittle polymer matrix and to initiate shear bands in the semiductile polymer matrix, which are responsible for the enhanced energy absorption.[1,4–7,15] The most important conclusion of these earlier studies was reached by Wu,[4,6,7] who demonstrated that the key parameter for rubber toughening is the thickness of the matrix ligaments between rubber particles. Recently, Muratoglu et al.[8–11] proposed a new morphological explanation of Wu's observations, in which the toughening effect of the dispersed particles is attributed to the changes in the matrix morphology (crystallographic texture) induced by the second-phase particles. Although many experimental phenomena can seemingly be explained by these mechanisms, the dependence of the impact strength and brittle–tough transition of

Correspondence to: Y. Zhang (zycnjuct@jlonline.comx).
Contract grant sponsor: Special Funds for Major State Basic Research Projects of China; contract grant number: G1999064809.
Contract grant sponsor: Nature Science Foundation of Jiangsu Province; contract grant number: BK93120406.

Journal of Applied Polymer Science, Vol. 87, 2120–2129 (2003)

those materials on their interfacial adhesion, matrix molecular weight, and crystallinity have not been reasonably examined.

In addition, there have been some articles about the effect of matrix shrinkage stress produced by the molding process on the crystalline structure and mechanical properties of polymers or polymer composites, in which the effect is proven to be the key factor for determining the reinforcing and toughening efficiency.[17–21] However, the proposed mechanisms do not consider it.

In this study, a series of high-density polyethylene (HDPE)/$CaCO_3$ blends were prepared with different kinds of coupling agents, with $CaCO_3$ particles of different sizes, and with matrices of different molecular weights. The effect of the interfacial stress produced by matrix shrinkage in the molding process on the matrix crystallinity, crystalline structure, and mechanical properties of the HDPE/$CaCO_3$ blends were studied. The toughening mechanism was examined.

EXPERIMENTAL

Materials

HDPE was obtained from Yang Zi Petrochemical Co. [5000F, melt index = 0.35 g/10 min, density = 0.955 g/cm^3; 3300F(1), melt index = 1.0 g/10 min, density = 0.954 g/cm^3; and 3300F(2), melt index = 1.14 g/10 min, density = 0.954 g/cm^3] and Union Carbide Co. (DGDY6098, melt index = 0.08 g/10 min, density = 0.953 g/cm^3). Three types of $CaCO_3$ were used: (A) average particle size = 3.2 μm and standard deviation = 1.1 μm, (B) average particle size = 4.6 μm and standard deviation = 2.3 μm, and (C) average particle size = 11.3 μm and standard deviation = 7.9 μm. The coupling agents were isopropyl trioleyl titanate (OLT951); isopropyl tri(dioctylpyrophosphato)titanate (NDZ); and an oxazoline-terminated polyether with a molecular weight of about 3000 (ON330), which was synthesized in our laboratory; its molecular formula is as follows:

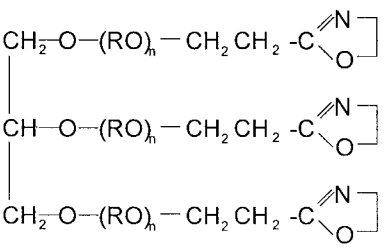

where R is

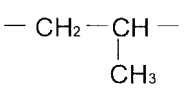

or

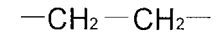

Sample preparation and mechanical property measurements

The $CaCO_3$ particles were dried at approximately 120°C for 2 h and then treated with an approximately 30% isopropyl alcohol coupling agent solution in a superspeed mixer. The volatile composition was removed in vacuo before the blending. The blends were prepared by melt mixing on a twin roller at 140–160°C, processed into sheets, and granulated. The samples for measuring the mechanical properties were prepared by injection molding at 210°C under a pressure of 50 MPa. The Charpy notched bar for impact testing was 120 × 15 × 10 mm^3, and the dumbbell-shaped bar for tensile testing was 4 mm thick. The bar for flexural testing and heat resistance testing was 120 × 15 × 10 mm^3. The samples from HDPE DGDY6098 were prepared via press molding at 160°C under a pressure of 10 MPa and then were machined in the form of bars.

The Charpy notched impact strength was measured according to GB1043-93 (Chinese standard) with an XGJ-5000 impact tester. The tensile and flexural tests were carried on a XL-100 tensile tester according to GB1040-92 and GB1042-79, respectively. The heat distortion temperature (under a 0.63-MPa load) of the blend was tested with an RW-1 heat resistance tester according to GB1634-79. All the tests were performed at room temperature (~23°C).

Measurement of the $CaCO_3$ particle size and its distribution

The $CaCO_3$ particle size and its distribution were measured with a centrifugal particle size measurer (SR-CP3, Japan).

Infrared spectra of $CaCO_3$

About 0.2 g of the blend was enclosed in a filter paper bag and extracted with xylene for 48 h. The residual $CaCO_3$ powders were dried in vacuo and then pressed into pellets with KBr. The testing was carried out with a Nicolet Magna IR 170XS spectrometer.

Differential scanning calorimetry (DSC)

The measurements were performed with a CDR-1 instrument (China). The specimens were heated to approximately 180°C at a constant rate of 10°C/min and were maintained for 5 min at this temperature; they were then cooled at a constant cooling rate of 1.0, 2.0,

TABLE I
Mechanical Properties of HDPE/$CaCO_3$ Blends and Their Dependence on $CaCO_3$ Surface Treatment and $CaCO_3$ Particle Size and Its Distribution

Sample	$CaCO_3$				Charpy impact strength (kJ/m^2)	Flexural strength (MPa)	Tensile strength (MPa)	Heat distortion Temperature (°C)
	Average diameter (μm)	Standard deviation	Content (mass %)	Surface treatment agent				
HDPE			0		18.6	38.8	23.8	65.0
A-30(a)	3.2	1.1	30	Untreated	20.8	33.9	20.2	83.0
B-30(a)	3.2	1.1	30	OLT951	43.9	33.5	20.1	83.5
C-30(a)	3.2	1.1	30	NDZ	44.8	32.5	17.5	83.5
D-30(a)	3.2	1.1	30	NDZ–ON330	50.6	32.9	18.3	84.5
D-30(b)	4.6	2.3	30	NDZ–ON330	41.5	29.3	17.0	81.0
D-30(c)	11.3	7.9	30	NDZ–ON330	10.3	27.7	17.0	79.5

Matrix: HDPE 3300F(1), Melt index = 1.0 (g/10 min).

5.0, or 10°C/min to 90, 70, 50, or 30°C, respectively. The crystallization enthalpies of the blend matrices were obtained and represented by ΔH_{C1}, ΔH_{C2}, ΔH_{C3}, and ΔH_{C4}, respectively.

Wide-angle X-ray diffraction (WAXD)

For a comparison of the effects of the cooling rate on the crystallization of the blend matrix, two different measured planes, which were 1.2 and 3.7 mm away from the surface of the injection-molded specimen (10 mm thick), were chosen through the mechanical cutting and grinding of the surfaces of the specimen. The WAXD scans were performed in the 2θ interval from 10 to 50° with graphite-filtered Cu Kα radiation (40 kV and 50 mA) with a Rigaku Rotaflex D/MAX-rA instrument. The diffraction intensities of the 001 reflection on the planes that were 1.2 and 3.7 mm away from the surface of the specimen were represented by $(I)_{1.2}$ and $(I)_{3.7}$, respectively; the sums of the diffraction intensities of the 110, 200, and 001 reflections on the planes 1.2 and 3.7 mm away from the surfaces of the specimen were represented by $(\Sigma I_i)_{1.2}$ and $(\Sigma I_i)_{3.7}$, respectively.

Scanning electron microscopy (SEM)

The impact fracture surfaces of the blends were immersed and etched for 4 h at 80°C with xylene to wash out the amorphous phase of HDPE on the surfaces of samples, and they were then dried in vacuo and observed with a scanning electron microscope (SX-40, Kashi, Japan). Some samples were fractured at the temperature of liquid N_2 and then etched with xylene.

RESULTS AND DISCUSSION

Mechanical properties of the HDPE/$CaCO_3$ blends

The mechanical properties of the HDPE/$CaCO_3$ blends and their dependence on the $CaCO_3$ surface treatment, the $CaCO_3$ particle size, and its distribution are shown in Table I. The Charpy notched impact strength of specimen A-30(a), in which the $CaCO_3$ particle surface was not treated, was close to that of HDPE; the impact strengths of specimens B-30(a) and C-30(a), in which the $CaCO_3$ surfaces were treated with OLT951 and NDZ (TTOPP-38S), respectively, were markedly increased. The impact strength of specimen D-30(a), in which the $CaCO_3$ surface was treated with the compounded coupling agent NDZ–ON330, was further enhanced.

Meanwhile, the heat distortion temperatures of specimens A-30(a), B-30(a), C-30(a), and D-30(a) were also slightly increased in order with different kinds of $CaCO_3$ surface-treatment agents, but the changes in the flexural and tensile strengths of these specimens were not obvious.

Figure 1 provides the Fourier transform infrared (FTIR) spectra of residual $CaCO_3$ from the extracted specimen by xylene. Curve 1 is the same as that of the pure $CaCO_3$ particles. In curve 2, two weaker peaks

Figure 1 FTIR spectra of $CaCO_3$ surfaces: (1) HDPE/$CaCO_3$ (untreated), (2) HDPE/$CaCO_3$ (NDZ-treated), and (3) HDPE/$CaCO_3$ (NDZ–ON330-treated).

appear near 1080 and 1020 cm^{-1}, which represent the absorbed bands of P═O and P—O—C groups, respectively, indicating the presence of stronger interfacial interactions between the coupling agent NDZ and the $CaCO_3$ surface in specimen C-30(a). In curve 3, two broad absorbed peaks appear near 1110 and 990 cm^{-1}, showing the presence of the absorbed bands of the ether (C—O—C) group in ON330, and the intensity of the absorbed peak near 1080 cm^{-1} was weakened. This phenomenon was attributed to the occurrence of the chemical reaction of the oxazoline groups (—$CNOC_2H_4$) of ON330 with the pyrophosphoric acid (—POOH—) groups of NDZ in the compounded coupling agent during the melt-mixing process. This chemical reaction led to the formation of the covered layer of ON330 soft molecular chains on $CaCO_3$ particles; therefore, ON330 on the $CaCO_3$ particle surfaces could not be extracted completely. Meanwhile, the ON330 molecular chains had to entangle or twine with the matrix molecular chains around $CaCO_3$ particles during the formation of the covered layer, further improving the interfacial adhesion of the blend. The $CaCO_3$ particles treated with a compounded coupling agent had, therefore, a better toughening action than the $CaCO_3$ particles treated only with NDZ or OLT951.

The data listed in Table I show that under the same surface-treatment conditions, the smaller the $CaCO_3$ particle was and the narrower its size distribution was, the higher the impact strength was of the blends. The flexural strength, the tensile strength, and the heat distortion temperature of these blends also gradually increased with decreasing $CaCO_3$ particle size and particle size distribution.

As shown in Figure 2, the Charpy notched impact strength of the blends was lower than or close to that

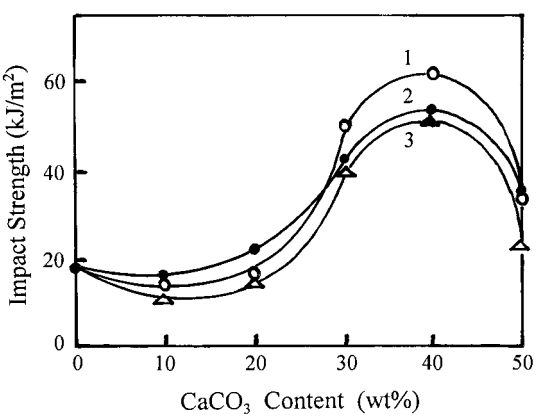

Figure 2 Charpy notched impact strength of the HDPE 3300F(1)/$CaCO_3$ blends versus the $CaCO_3$ content: (1) $CaCO_3$, d = 3.2 μm, S = 1.1 μm, surface-treated with NDZ–ON330; (2) $CaCO_3$, d = 3.2 μm, S = 1.1 μm, surface-treated with OLT951, and (3) $CaCO_3$, d = 4.6 μm, S = 2.3 μm, surface-treated with NDZ–ON330.

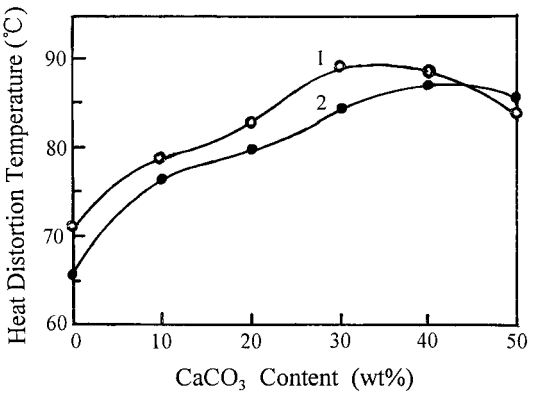

Figure 3 Heat distortion temperature of the HDPE/$CaCO_3$ blends versus the $CaCO_3$ content: (1) HDPE 5000F and (2) HDPE 3300F(1) ($CaCO_3$, d = 3.2 μm, S = 1.1 μm, surface-treated with NDZ–ON330).

of HDPE when the $CaCO_3$ content was less than 20%. However, the impact strength increased quickly, and the specimens exhibited a brittle–tough transition behavior when the $CaCO_3$ content was greater than 20%; the impact strength of the blends with 40% $CaCO_3$ reached a maximum (62.0 kJ/m^2, curve 1). Comparing curves 1 and 2, one can see that the toughening action of the $CaCO_3$ particles treated with a compounded coupling agent was better than that of the particles treated with a single coupling agent. Comparing curves 1 and 3, one can see that the toughening action of the $CaCO_3$ particles with smaller particle sizes and particle size distributions was better than that of the particles with bigger particle sizes and particle size distributions.

Figure 3 shows the heat distortion temperatures of the blends and their dependence on the $CaCO_3$ content. The heat distortion temperatures obviously increased with an increase in the $CaCO_3$ content and reached maxima at 30 (curve 1) and 40% (curve 2) $CaCO_3$.

Analysis of the DSC data

As shown in Figure 4, the crystallization enthalpy ΔH_C of the blend matrix did not obviously change with increasing $CaCO_3$ content when the cooling rate of the tested specimen was slow, as for curve 1 (cooling rate = 1°C/min). However, ΔH_C obviously changed when the cooling rate of the tested specimen was increased, as for curves 2–4 (cooling rate = 2, 5, and 10°C/min, respectively). For example, when the $CaCO_3$ content was less than 20%, the values of ΔH_C did not obviously change, but when the $CaCO_3$ content was greater than 20%, they obviously increased with increasing $CaCO_3$ content. A faster cooling rate of the specimen melt could lead to a quicker increase in ΔH_C, and the values of ΔH_C also reached a maximum at 40% $CaCO_3$. All these patterns agreed with those of the

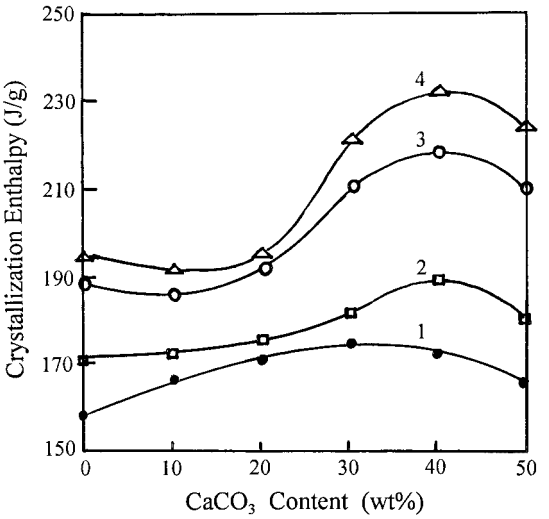

Figure 4 Matrix crystallization enthalpy of the HDPE 3300F(1)/$CaCO_3$ blends at different cooling rates (a) versus the $CaCO_3$ content: (1) a = 1.0°C/min, (2) a = 2.0°C/min, (3) a = 5.0°C/min, and (4) a = 10.0°C/min ($CaCO_3$, d = 3.2 μm, S = 1.1 μm, surface-treated with NDZ–ON330).

impact strengths of the blends, showing an S-type curve variation.

Figure 5 shows that the values of ΔH_C of the blend matrix also increased in order with the changes in the $CaCO_3$ surface coupling agents, as for curves 1–4. At the same time, with an increase in the cooling rate of the tested specimens, the values of ΔH_C also obviously increased. However, for curves 1–3, the values of ΔH_C obviously decreased when the cooling rate was greater than or equal to 7°C/min because of their weaker interfacial adhesion. The variation of ΔH_C with different kinds of coupling agents between cooling rates of 5 and 9°C/min was also identical to that of the impact strength of the corresponding blends.

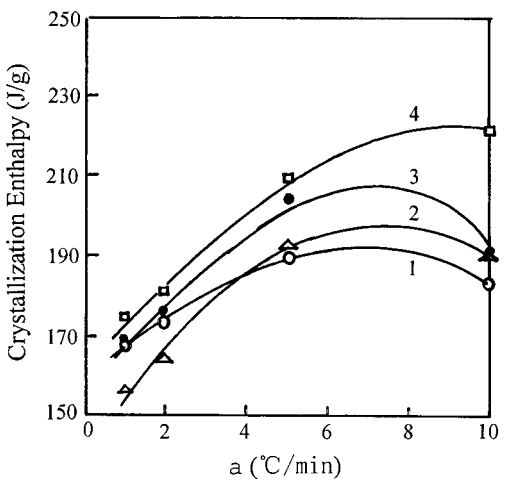

Figure 5 Matrix crystallization enthalpy versus the cooling rate (a) of the specimens: (1) specimen A-30(a), (2) specimen B-30(a), (3) specimen C-30(a), and (4) specimen D-30(a).

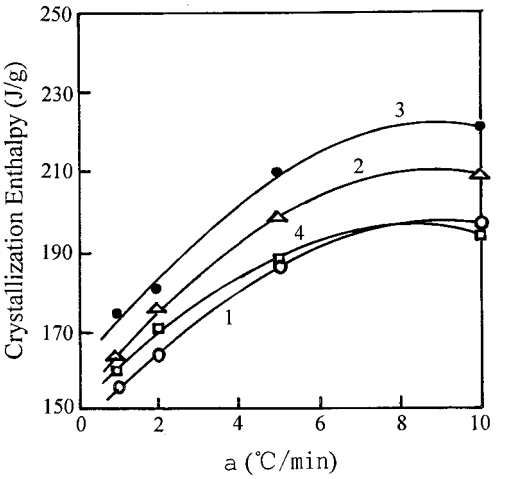

Figure 6 Matrix crystallization enthalpy versus the cooling rate (a) of the specimens: (1) specimen D-30(c), (2) specimen D-30(b), (3) specimen D-30(a), and (4) HDPE 3300F(1).

As shown in Figure 6, ΔH_C increased with a decrease in the $CaCO_3$ particle size and its size distribution and with an increase in the cooling rate of the specimen melts, and this also agreed with the variation tendency of the impact strengths of the blends.

This consistency of the variation tendency of the matrix crystallinity with that of the impact strength of the blends and their dependence on the matrix crystalline morphology were further investigated with HDPE/GF and HDPE/filler blends.[18–21] The experimental results indicated that the interfacial stress coming from the blend molding process resulted in the strain-induced crystallization of the matrix and led to the formation of the extended-chain (or microfibrillar) crystal layers on the interfacial surface and their extension in the matrix. The impact strength of the blends and the matrix crystallinity were, therefore, obviously influenced. As for the HDPE/$CaCO_3$ blends with higher interfacial adhesion, the interfacial stress produced by the matrix shrinkage during the molding process caused the drawing and orientation of the molecular chains in the matrix surrounding the $CaCO_3$ particles and induced crystallization of the chains, leading to the formation of the interfacial transition region, which consisted of the extended-chain (or microfibrillar) crystal layers.[18–21] A higher $CaCO_3$ content and a smaller $CaCO_3$ particle size could produce a more average distribution of the interfacial stress and a closer distance between $CaCO_3$ particles and lead to the formation of a higher proportion of the extended-chain (or microfibrillar) crystal in the matrix. For the blends with a smaller $CaCO_3$ particle size and a higher $CaCO_3$ content, the strain-induced areas or the interfacial transition regions among the $CaCO_3$ particles overlapped or connected with one another. In this case, the microvolume element of this matrix among the different $CaCO_3$ particles could be drawn

and strained by the interfacial stress from different directions, resulting in the enhancement of the strain-induced crystallization and an obvious increase in the matrix crystallinity. The faster the cooling rate was, the higher the shrinkage stress was of the matrix, and the stronger the effect was of the strain-induced crystallization. For a stronger effect of the strain-induced crystallization, the extended-chain (or microfibrillar) crystal layers among the different $CaCO_3$ particles connected with one another and fully filled the matrix, leading to the formation of the extended-chain (or microfibrillar) crystal network structure. Consequently, the impact strength of the blend and its matrix crystallinity were obviously increased when the $CaCO_3$ particles were treated with a compounded coupling agent of NDZ and ON330, and the particle size and distribution were smaller when the content was greater than 20%. Under these conditions, the blends showed a transition from brittle fracture behavior to tough fracture behavior.

By contrast, the interfacial stress produced by the matrix shrinkage during the blend molding process could be released by the debonding of the interfacial phase and the formation of the interfacial cracks if the interfacial adhesion force was weaker or the $CaCO_3$ particle size was larger. Therefore, under these conditions, the extended-chain (or microfibrillar) crystal layers and their network structure could not be formed. This was the main reason that both the impact strengths of blend specimens A-30(a) and D-30(c) and their matrix crystallinities were much lower.

WAXD analysis

As the data listed in Table II show, despite the different interfacial adhesions, the different $CaCO_3$ contents, and the different particle sizes in the blends, the d values of the 110 and 200 reflections were the same. This indicated that the orthorhombic system of the HDPE matrix was not altered. However, there was a weak peak at $2\theta = 19.4°$ in the recorded meridional diffractogram curve, and its relative difference value of the diffraction intensity on two different planes, $[(I)_{1.2} - (I)_{3.7}]/(I)_{1.2}$, obviously varied with the $CaCO_3$ content, interfacial adhesion, and $CaCO_3$ particle size. These changes were caused by the different cooling rates on the two different planes (1.2 and 3.7 mm distant from the surfaces of the specimens). For example, with an increase in the $CaCO_3$ contents in the blends, such as for specimens D-0 and D-10(a) to D-50(a), the $[(I)_{1.2} - (I)_{3.7}]/(I)_{1.2}$ value of this peak also showed an S-type curve variation and reached a maximum at a $CaCO_3$ content of 40%. With an increase in the interfacial adhesion [specimens A-30(a) to D-30(a)] or a decrease in the $CaCO_3$ particle size and its distribution [specimens D-30(c), D-30(b), and D-30(a)], the $[(I)_{1.2} - (I)_{3.7}]/(I)_{1.2}$ values of this peak also increased. The peak at $2\theta = 19.4°$ corresponded to the diffraction peak of the monoclinic crystals induced by the interfacial stress.[22,23] This phenomenon indicated that the monoclinic crystal proportion also increased with an increase in the interfacial adhesion force, the $CaCO_3$ content, and the cooling rate of the molten specimens or with a decrease in the $CaCO_3$ particle size and its distribution.

Moreover, the relative difference value of the total diffraction intensity on two different planes $[(\Sigma I_i)_{1.2} - (\Sigma I_i)_{3.7}]/(\Sigma I_i)_{1.2}$, also varied with the interfacial adhesion, the $CaCO_3$ content, and its particle size because of the different cooling rates of the specimens on the two different planes. Comparing specimens D-0, D-10(a), D-20(a), D-30(a), D-40(a), and D-50(a), we found that the total diffraction intensity of the three peaks $(\Sigma I_i)_{1.2}$ or $(\Sigma I_i)_{3.7}$ decreased in order because of the dilution action of $CaCO_3$ particles, but the $[(\Sigma I_i)_{1.2} - (\Sigma I_i)_{3.7}]/(\Sigma I_i)_{1.2}$ values also varied obviously according to the S-type curve variation. When the interfacial adhesion was weak or the $CaCO_3$ particle size was large, such as for specimens A-30(a), B-30(a), C-30(a), and D-30(c), their $[(\Sigma I_i)_{1.2} - (\Sigma I_i)_{3.7}]/(\Sigma I_i)_{1.2}$ values became lower or negative. However, in the other compositions, these values showed obvious increases. These results were consistent with the results of the DSC analysis. Because of the effect of the interfacial stress on strain-induced crystallization, the matrix crystalline structure and texture of these blends were obviously changed, and these changes led to the obvious change in the matrix crystallinity of the blends.

Dependence of the impact strength of the HDPE/$CaCO_3$ blends on their matrix molecular weights

Figure 7 shows that the HDPE matrix with a higher molecular weight caused an earlier occurrence of the brittle–tough transition of the blends and reached a higher and earlier maximum on the Charpy notched impact strength curve. As with an increase in the matrix molecular weight or a decrease in the melt index of HDPE, the brittle–tough transitions of the blends (curves 3–1) occurred at about 35, 30, and 20% $CaCO_3$ contents, respectively, and the impact strengths reached the maximum at 43, 40, and 30% $CaCO_3$ contents, respectively. The maximum value of the impact strength became higher, and the toughening action of the $CaCO_3$ particles became better.

According to the theory concerning the criterion of the critical matrix ligament thickness (T_C; or the critical surface-to-surface interparticle distance),[4–7] these phenomena showed that under the same conditions, the higher the matrix molecular weight was, the larger the T_C value was of the blends. However, if the brittle–tough transition depended on the number of defined interactions of stress concentration fields around spherical particles, which were induced from extra

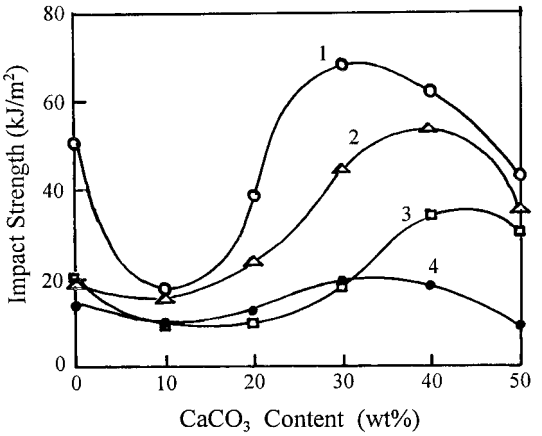

Figure 7 Charpy notched impact strength of the HDPE/$CaCO_3$ blends with different HDPE matrix molecular weights versus the $CaCO_3$ content: (1) HDPE 5000F, melt index = 0.35 g/10 min; (2) HDPE 3300F(1), melt index = 1.0 g/10 min; (3) HDPE 3300F(2), melt index = 1.14 g/10 min; and (4) HDPE DGDY6098, melt index = 0.08 g/10 min ($CaCO_3$, d = 3.2 μm, S = 1.1 μm, surface-treated with OLT951).

force,[4–7] or if the T_C value was determined by second-phase nucleation,[8–11] this kind of varying regulation of T_C could not be explained.

According to the theory concerning the effect of interfacial stress on strain-induced crystallization,[18–21] these phenomena could be explained reasonably. When the matrix molecular weight became higher, the interaction force between the molecule chains was increased, and the strain-induced areas or interfacial transition regions became wider; this meant that the extended-chain (or microfibrillar) crystal layers became thicker or that the extended-chain (or microfibrillar) crystal spheres became larger. The thicker extended-chain crystal layers or the larger extended-chain crystal spheres could, therefore, connect with one another at lower $CaCO_3$ contents and form more connections among themselves. Therefore, they could form the extended-chain crystal network structure in the blend earlier. This was the key reason that the brittle–tough transition and the maximum impact strength of the blends could occur at a lower $CaCO_3$ content as the molecular weight of the matrix was increased.

Curve 4 in Figure 7 shows the relationship between the impact strength of HDPE DGDY6098/$CaCO_3$ blends and their $CaCO_3$ content. Although the maximum impact strength was reached at a lower $CaCO_3$ content, the maximum was less, and the efficiency of the toughening action of the $CaCO_3$ particles was low. In addition, DSC data showed that ΔH_C of HDPE DGDY6098 (ΔH_{C3} = 174 J/g, ΔH_{C4} = 183 J/g) was obviously lower than that of HDPE 5000F (ΔH_{C3} = 197 J/g, ΔH_{C4} = 196 J/g) or HDPE 3300F (ΔH_{C3} = 188 J/g, ΔH_{C4} = 194 J/g). This indicated that, besides the matrix molecular weight, the regularity and crystallinity of the matrix molecule chains were also key factors influencing the strain-induced crystallization and the toughening efficiency.

Dependence of the tensile strength and Young's modulus of the HDPE/$CaCO_3$ blends on the $CaCO_3$ contents and particle sizes

As shown in Figure 8, the tensile strength of the blend was slightly decreased with an increase in the $CaCO_3$ content. The larger the $CaCO_3$ particle size was, the more obvious the decrease was in the tensile strength. However, this was not true for Young's modulus of the blend. When the $CaCO_3$ content was 0–20%, Young's modulus was about 1000 MPa, and it then quickly increased up to a 40% $CaCO_3$ content (ca. 2070 MPa, curve 4); over the 40% $CaCO_3$ content condition, this rise became slow. The smaller the $CaCO_3$ particle size was, the more obvious the increase was in the modulus. This phenomenon also indicated that besides the reinforcing action of $CaCO_3$ particles, the strain-induced crystallization action, the increase in the matrix crystallinity, and the formation of the extended-chain crystal network also played very important roles in the increase in the Young's moduli of the blends.

Fracture morphology

Figure 9 shows the SEM micrographs of the impact-fractured surfaces of the specimens. Interfacial gaps

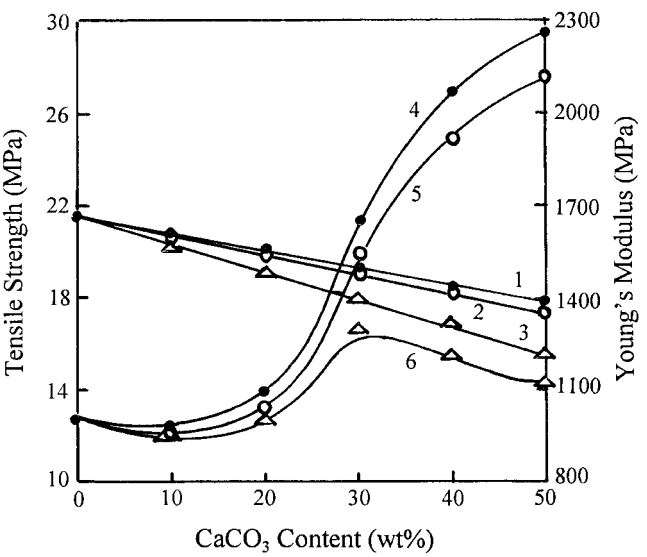

Figure 8 Tensile strength and Young's modulus of HDPE 3300F(1)/$CaCO_3$ blends of different $CaCO_3$ particle sizes versus the $CaCO_3$ content: (1,4) $CaCO_3$, d = 3.2 μm, S = 1.1 μm; (2,5) $CaCO_3$, d = 4.6 μm, S = 2.3 μm; and (3,6) $CaCO_3$, d = 11.3 μm, S = 7.9 μm ($CaCO_3$, surface-treated with NDZ–ON330).

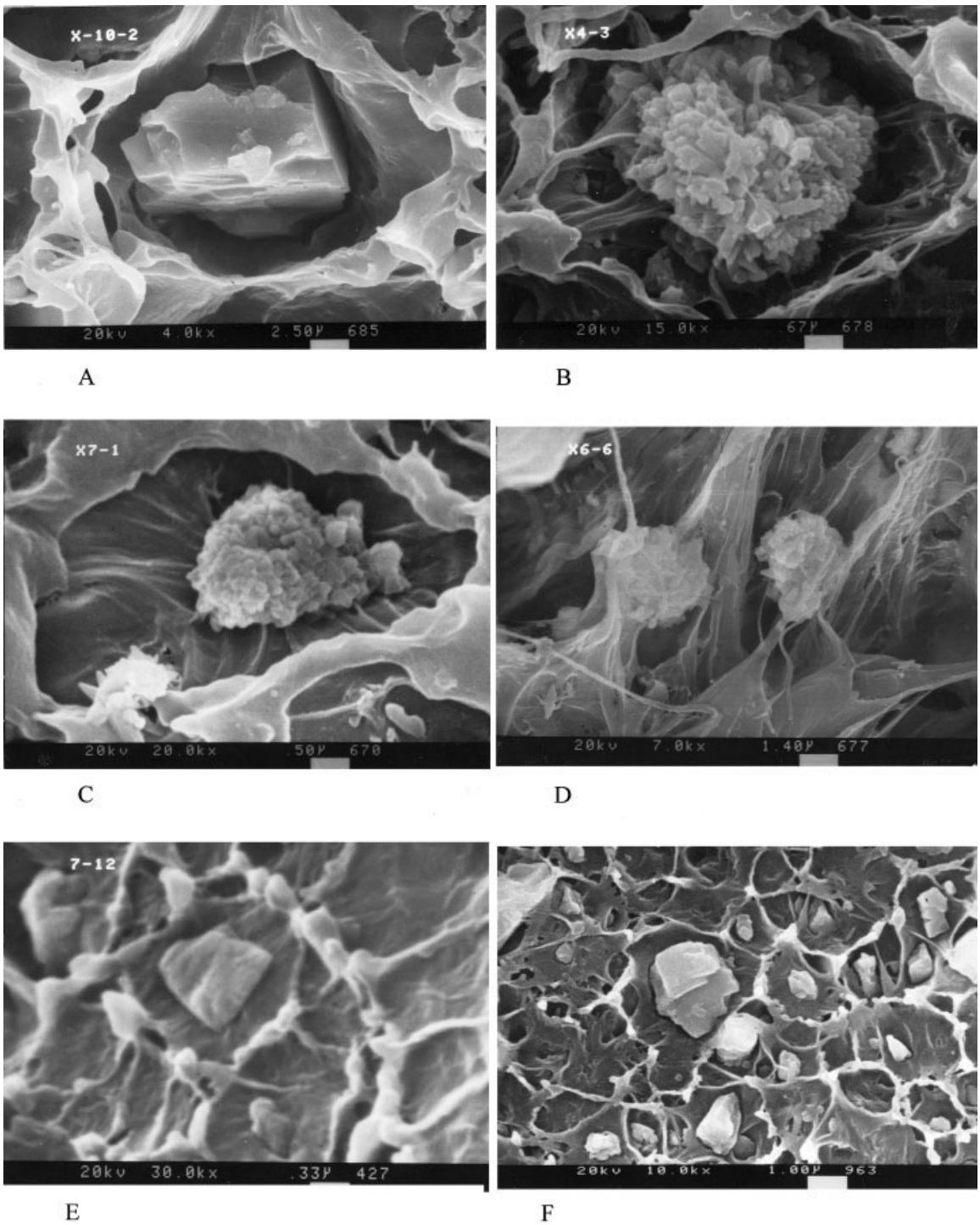

Figure 9 SEM micrographs of the specimens: (A) specimen D-30(c), 30% $CaCO_3$; (B) specimen A-30(a), 30% $CaCO_3$; (C) specimen D-10(a), 10% $CaCO_3$; (D) specimen D-30(a), 30% $CaCO_3$; (E) 10% $CaCO_3$, d = 1.61 μm, S = 1.05 μm; and (F) 30% $CaCO_3$, d = 1.61 μm, S = 1.05 μm (the fractured specimen surfaces were etched with xylene for 4 h at 80°C; parts E and F are images of liquid-nitrogen-frozen fractured surfaces).

between the $CaCO_3$ particles and matrix can be seen in Figure 9(A,B) because of the larger $CaCO_3$ particles in specimen D-30(c) and the weaker interfacial adhesion in specimen A-30(a), for which the $CaCO_3$ particle surface was not treated. Figure 9(C) [specimen D-10(a)], Figure 9(E), and Figure 9(F) show that the $CaCO_3$ particles were strongly bonded to the matrix when the $CaCO_3$ particle size was rather small and its surface was well treated with a compounded coupling agent. The matrix around the $CaCO_3$ particles showed a radiative streak line structure that consisted of the extended-chain (or microfibrillar) crystal layers.[20,21]

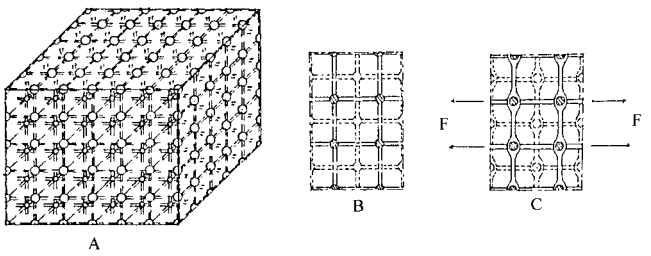

Figure 10 Model of the extended-chain crystal network.

The radiative streak line regions around the $CaCO_3$ particles connect with one another in Figure 9(F), and this means that the extended-chain crystal transition layers among the $CaCO_3$ particles connected with one another and constituted the extended-chain crystal network in the matrix. These are the major reasons that the blends showed the transition from brittle fracture behavior to tough fracture behavior.

Figure 9(D) shows the classic toughening fracture pattern of specimen D-30(a). The specimen matrix had some vacancies; the fibrous crystals were drawn and elongated.

Model proposal

An extended-chain crystal network model is proposed. It is supposed that two sets of $CaCO_3$ particles, which are put in a cubic type, interpenetrate each other to form a cubic network (Fig. 10). The extended-chain crystal layers around $CaCO_3$ particles are represented by a series of double-X lines to express the extended-chain crystal layers, which are perpendicular to one another; the extended-chain crystal layers in the other direction are neglected. There are a few connections between the parallel extended-chain crystal layers due to the directivity of the extended-chain crystal layers, and their bond strength is fairly weak. When the blend is subjected to impact, the extended-chain crystal layers (the oriented planes of which are perpendicular to the direction of the subjected force) will crack along the center planes of the $CaCO_3$ particles. As shown in Figure 10(B,C), many crazes will be induced along the center planes of the $CaCO_3$ particles. Meanwhile, the extended-chain crystal layers (the oriented planes of which are parallel to the direction of the subjected force) enhance the bond strength between the cracking planes and restrain the further cracking of these crazes. This means that the extended-chain crystal network both induces many crazes and limits the further cracking of these crazes when the blend is impacted. However, the extended-chain crystal layers (the oriented planes of which are parallel to the direction of the subjected force) will be elongated and appear as plastic deformation under the higher external impact force because they are distributed in the HDPE amorphous phase. When the two actions take place simultaneously, the matrix will produce many crazes and plastic deformation and absorb a lot of impact energy. This is the main reason that the HDPE/$CaCO_3$ blends show the transition from brittle fracture behavior to tough fracture behavior and a higher impact strength under certain conditions.

Meanwhile, the formation of the extended-chain crystal network and its density increase also increase the crystallinity of the matrix and enhance the connection among the $CaCO_3$ particles. This is the main reason that the heat distortion temperature and Young's modulus of the blends are obviously increased.

CONCLUSIONS

During the melt-mixing process of HDPE and $CaCO_3$ particles, ON330 reacted with NDZ in a compounded coupling agent, and this led to the formation of the covered layer of ON330 soft molecular chains on $CaCO_3$ particles and obviously improved their interfacial adhesion. In this case, the Charpy notched impact strength of the blend (60/40) was 62.0 kJ/m^2, 2.3 times higher than that of unimproved HDPE, and its Young's modulus was 2070 MPa, 1.07 times higher than that of unimproved HDPE. The heat distortion temperature of the blend was also obviously increased.

The improvement of the mechanical properties and the occurrence of the brittle–tough transition of the blends were due to the crystallization effect induced by the interfacial stress. With higher interfacial adhesion and with more than 30% $CaCO_3$, the interfacial stress produced from the matrix shrinkage in the blend molding process could strain-induce crystallization of the matrix, leading to an increase in the matrix crystallinity and the formation of the extended-chain crystal network. The interfacial adhesion and the $CaCO_3$ particle size, particle size distribution, and content, as well as the cooling rate of the specimen melts in the molding process, were the key factors determining the formation of the extended-chain crystal network structure.

A higher molecular weight HDPE matrix caused the occurrence of the brittle–tough transition and a higher maximum of the impact strength of the blends at a lower $CaCO_3$ content, and this implied that the material T_C became larger. This phenomenon was attributed to the strain-induced areas becoming wider, the extended-chain crystal layers becoming thicker, and the interparticle distance that formed the extended-chain crystal network structure becoming larger with a higher matrix molecular weight. Meanwhile, the regularity and crystallinity of the matrix molecule chains were also key factors influencing the strain-induced crystallization and determining the toughening efficiency.

The formation of the extended-chain crystal network and the increase in the matrix crystallinity in the blends were also important reasons that the heat distortion temperature and Young's modulus of the blends increased.

References

1. Bucknall, C. B. Toughened Plastics; Applied Science: London, 1977.
2. Flexman, E. A. Polym Eng Sci 1979, 19, 564.
3. Jang, B. Z.; Uhlman, D. R.; Vander Sande, J. B. J Appl Polym Sci 1984, 29, 3409.
4. Wu, S. J Polym Sci Polym Phys Ed 1983, 21, 699.
5. Hobbs, S. Y.; Bopp, R. C.; Watkins, V. H. Polym Eng Sci 1983, 23, 1983.
6. Wu, S. Polymer 1985, 26, 1855.
7. Wu, S. J Appl Polym Sci 1988, 35, 549.
8. Muratoglu, O. K.; Argon, A. S.; Cohen, R. E. Polymer 1995, 36, 921.
9. Bartczak, Z.; Argon, A. S.; Cohen, R. E.; Weinberg, M. Polymer 1999, 40, 2331.
10. Bartczak, Z.; Argon, A. S.; Cohen, R. E.; Weinberg, M. Polymer 1999, 40, 2347.
11. Bartczak, Z.; Argon, A. S.; Cohen, R. E.; Kowalewski, T. Polymer 1999, 40, 2367.
12. Kurauchi, T.; Ohta, T. J Mater Sci 1984, 19, 1669.
13. Koo, K. K.; Inoue, T.; Miyasaka, K. Polym Eng Sci 1985, 25, 741.
14. Angola, J.; Fujita, Y.; Sakai, T.; Inoue, T. J Polym Sci Part B: Polym Phys 1988, 26, 807.
15. Fu, Q.; Wang, G. Polym Eng Sci 1992, 32, 94.
16. (a) Chin. Pat. ZL 95111154.X; (b) Chin. Pat. ZL 95112772.1.
17. Galeskl, A.; Piorkowska, E.; Koenczoel, L.; Baer, E. J Polym Sci Part B: Polym Phys 1990, 28, 1171.
18. Zhang, Y.; Chen, R.; Yu, J. Polym Mater Sci Eng (China) 1992, 8, 94.
19. Zhang, Y.; Xing, H.; Chen, R. Polym Mater Sci Eng (China) 1992, 8, 95.
20. Zhang, Y.; Cheng, R.; Zhang, S. Acta Mater Compos Sinica (China) 1996, 13(3), 12.
21. Zhang, Y.; Chen, R.; Hui, Z. J Adhes Sci Technol 2000, 14, 1405.
22. Zhang, C. M. Acta Polym Sinica (China) 1997, No. 1, 31.
23. Tsuneo, S.; Tetsuhiko, H.; Kenzo, T. Jpn J Appl Phys 1968, 7, 31.